

Effects of temperature, strain rate, and vacancies on tensile and fatigue behaviors of silicon-based nanotubes

Yeau-Ren Jeng,^{1,*} Ping-Chi Tsai,¹ and Te-Hua Fang²

¹*Department of Mechanical Engineering, National Chung Cheng University, Chia-Yi 621, Taiwan*

²*Department of Mechanical Engineering, Southern Taiwan University of Technology, Tainan 710, Taiwan*

(Received 5 April 2004; revised manuscript received 23 November 2004; published 11 February 2005)

This paper adopts the Tersoff-Brenner many-body potential function to perform molecular dynamics simulations of the tensile and fatigue behaviors of hypothetical silicon-based tubular nanostructures at various temperatures, strain rates, and vacancy percentages. The tensile test results indicate that with a predicted Young's modulus of approximately 60 GPa, silicon nanotubes (SiNTs) are significantly less stiff than conventional carbon nanotubes. It is observed that the presence of hydrogen has a significant influence on the tensile strength of SiNTs. Additionally, the present results indicate that the tensile strength clearly decreases with increasing temperature and with decreasing strain rate. Moreover, it is shown that the majority of the mechanical properties considered in the present study decrease with an increasing vacancy percentage. Regarding the fatigue tests, this study uses a standard theoretical model to derive curves of amplitude stress versus number of cycles for the current nanotubes. The results demonstrate that the fatigue limit of SiNTs increases with a decreasing vacancy percentage and with increasing temperature.

DOI: 10.1103/PhysRevB.71.085411

PACS number(s): 61.46.+w, 62.25.+g, 61.72.Qq, 65.80.+n

I. INTRODUCTION

Recent studies have reported the synthesis of nanotubes with various chemical compositions.^{1,2} The literature provides many discussions relating to the synthesis of $B_xC_yN_z$ three-component nanotubes,³⁻⁶ Mo and W chalcogenide nanotubes,⁷⁻⁹ vanadium oxide nanotubes,¹⁰ NiCl cage structures and nanotubes,¹¹ NiC_{12} nanotubes,¹² $H_2Ti_3O_3$ nanotubes,¹³ TiO_2 nanotubes,¹⁰ Y_2O_3 europium nanotubes,¹⁴ and rare earth oxide nanotubes.¹⁵ Theoretical GaN,¹⁶ GaSe,¹⁷ P,¹⁸ Cu,¹⁹ Bi,²⁰ B_2O , and BeB_2 (Ref. 21) nanotubes have also been reported. In the nanotechnology field, new forms of materials such as nanowires and nanotubes are now being used increasingly in place of silicon in the fabrication of electronic devices. Importantly, even though silicon and carbon are both isovalent, the manner in which they form chemical bonds is quite different. For example, in carbon, the sp^2 hybridization is more stable, while in silicon, the sp^3 hybridization is more stable. Consequently, carbon will readily form graphite, fullerene, and nanotubes composed predominantly with sp^2 bonds, whereas silicon adopt predominantly a diamond form. Nevertheless, the possible existence of silicon nanotubes (SiNTs) cannot be entirely discounted. Recently, many authors have investigated SiNTs. For example, Bahel and Ramakrishna²² revealed that the lowest energy structure of the Si_{12} cluster is a bicapped pentagonal antiprism, referred to as a hollow icosahedron. Menon and Richter²³ proposed a quasi-one-dimensional silicon structure, characterized by a core of bulklike fourfold-coordinated atoms surrounded by a structure of reconstructed surfaces formed primarily by threefold-coordinated atoms. Meanwhile, Marsen and Sattler²⁴ presented a model for silicon nanowires consisting of fullerene-like structures. In a further study,²⁵ a tight-binding molecular dynamics approach was used with the *ab initio* method to investigate the stabilization of Si cages by the encapsulation of the Ni chain.

Fagan *et al.*²⁶ discussed the significant costs involved in producing graphitelike sheets of silicon. Generally speaking, the majority of the computer-aided-investigations and experimental results discussed in the literature²⁷⁻³⁴ concern the basic mechanical properties of nanotubes and nanowires under axial compression or tension. The mechanical properties of SiNTs are important since potential applications depend on the stability and stiffness of the nanotubes. However, relatively few studies have attempted a detailed investigation of the full range of SiNT mechanical properties. Consequently, the present study employs classical molecular dynamics (MD) simulations based on the Tersoff-Brenner many-body potential function^{35,36} to perform a comprehensive investigation into the mechanical properties of promising silicon and silicon-based nanotubes.

II. METHODOLOGY

The present study adopts the Tersoff-Brenner many-body potential function^{35,36} to model the Si-Si and C-C interactions. This potential function describes the interatomic forces, the elastic properties, the molecular bond energies, and the bond lengths of the Si-Si structure. Although originally developed to study the chemical vapor deposition of diamond, this potential function is commonly applied in the modeling of fullerenes.³⁷ Recently, several researchers have successfully demonstrated its use in the modeling of a wide range of structural properties of a variety of materials, including carbon and silicon.²⁸⁻³⁰ Although it is acknowledged that the accuracy of the Tersoff-Brenner many-body potential function does not match that of quantum-mechanical methods, it is nevertheless adopted in the present simulations since it is simple, computationally inexpensive, and has been used successfully for similar purposes in previous studies. In order to validate the applicability of the Tersoff-Brenner potential to the investigation of low-dimensional nanostructures,

TABLE I. Selected measured and predicted mechanical properties of bulk cubic diamond Si and carbon along different orientations as obtained using Tersoff-Brenner potential.

Structure	Orientation	Poisson ratio	Critical strain (%)	Young's modulus (GPa)
Diamond Si	(100)	0.223	15.27	176.5
	(110)	0.247	19.39	165.8
	(111)	0.269	21.43	158.4
Diamond carbon	(100)	0.185	26.56	1067.2
	(110)	0.176	21.34	1134.5
	(111)	0.163	17.83	1178.3

tures, the present calculated values for the mechanical properties of bulk cubic diamond Si and carbon are compared with typical experimental and theoretical results. As shown in Table I, the Young's moduli of bulk cubic diamond Si are calculated to be 176.5, 165.8, and 158.4 GPa in the (100), (110), and (111) directions, respectively. It is clear that the Young's modulus is strongly dependent on the crystallographic direction. Our calculated values of bulk Si compare well with typical values in previous studies. For bulk silicon (100) and (110), the predicted Young's modulus varies from 130.2 GPa to 187.5 GPa.³⁸⁻⁴⁴ Lee *et al.* reported that Young's modulus for bulk silicon (111) is about 168.9 GPa.⁴⁵ The current results are in good agreement with the rather more precise theoretical estimates presented in the above studies. For diamond carbon, Table I reveals that the calculated Young's moduli between 1 and 1.2 TPa. Furthermore, it is observed that the critical strain of the diamond carbon attains its maximum value parallel to the (100) direction and its minimum value in the (111) direction. This tendency is in good agreement with the recent findings of Ansell *et al.* and O'Keefe *et al.*^{46,47} Although the present results for the Young's modulus are slightly different from the experimental and computational results presented previously,⁴⁸⁻⁵⁰ but that the adopted Tersoff-Brenner potential is nevertheless adequate for generating the current qualitative estimates. However, an important unresolved issue remains, namely the extent to which the results would be affected by the application of more robust potentials.

This study investigates the mechanical properties of two extreme hypothetical silicon nanotubes, i.e., the (10,10) and (17,0) SiNTs, having approximately equal radii of ~ 22.05 Å. The nanotubes comprise a pure silicon tube with a surface containing many polymeric syntheses.^{51,52} An assumption is made that polymeric synthesis takes place at the surfaces of the SiNT. Hence, the walls may become saturated with hydrogen (SiH). The Si-Si bond distances are calculated to be 2.245 Å (Refs. 53-57) while the Si-H bond length is determined to be 1.52 Å.⁵⁸ In the present tensile simulations, the nanotubes are initially annealed at a specified temperature over a period of 10^6 time-steps, where each step is separated by an interval of 0.5 fs. Periodic boundary conditions are imposed in the x and y directions, and the nanotubes are then extended axially (i.e., in the z direction) under the application of an appropriate strain [Fig. 1(a)]. The initial configuration of the molecular dynamics simulation for the fatigue test is shown in Fig. 1(b). The two ends of the

specimen, labeled as A, are assumed to be free motion regions within which velocity rescaling is applied. Meanwhile, the atoms in the central region of the specimen, labeled as B, are subjected to reverse uniaxial tension-compression loading in the z direction. It is noted that the loading cycles are always fully reversed such that the maximum compressive stress and the maximum tensile stress are equal. Conventional periodic boundary conditions are imposed in the x and y directions. The test specimens are cycled to their failure point, which in this study is defined as the point at which the specimen separates into two halves. In order to investigate the relative influences of thermal effects, strain rates, and vacancies on the mechanical properties of the current SiNTs under tension and fatigue loading conditions, this study simulates testing under various temperatures in the range of 300 K to 1500 K, with strain rates varying from 10^{-6} ps⁻¹ to 10^{-2} ps⁻¹ and vacancy percentages (V) ranging from 6% to 30%.

III. RESULTS AND DISCUSSION

A. Mechanical properties of silicon and Si-based nanotubes under tension

The present theoretical investigations of SiNTs are restricted primarily to the comparison and contrast of the mechanical behaviors of (10,10) and (17,0) SiNTs with those of carbon nanotubes of similar radii Fig. 2 presents the varia-

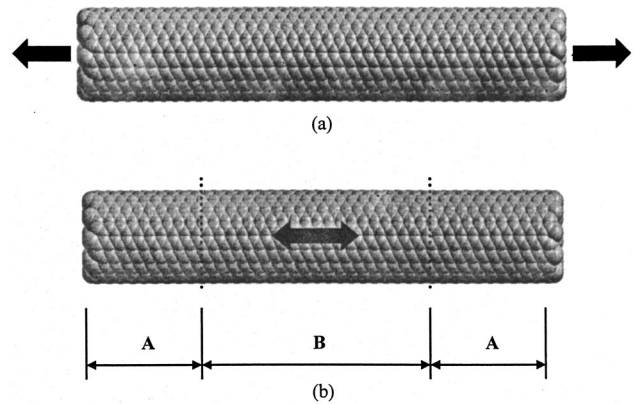


FIG. 1. Initial configuration of silicon nanotubes for (a) tensile test and (b) fatigue test. [Label "A" in (b) denotes the free motion region and "B" indicates the tension-compression region.]

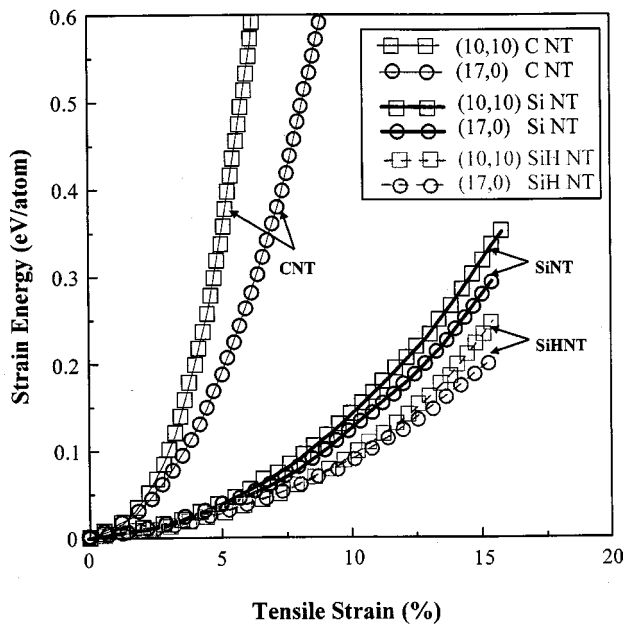


FIG. 2. Strain energy values of (10,10) and (17,0) Si (thick solid line), SiH (dotted line), and carbon (thin solid line) nanotubes as a function of the axial tensile strain.

tion of the strain energy per atom, which is calculated as the difference between the total energy per atom in the strained and unstrained conditions, with the percentage strain for these nanotubes. For reasons of clarity, in comparing the mechanical behaviors of the different tubes, Fig. 2 presents the results for the linear elastic response regime only. It is noted that the linear elastic response regime is limited to low applied strains ($\leq 8\%$) and is characterized by the absence of plastic structural deformation. The Young's modulus value for each nanotube is determined by applying a parabolic fit to the corresponding plotted data. The Young's modulus is calculated as the second derivative of the total energy with respect to the strain at the equilibrium configuration (i.e., at zero strain), i.e.,

$$Y = \frac{1}{V_0} \left(\frac{\partial^2 E}{\partial \epsilon^2} \right)_{\epsilon=0}, \quad (1)$$

TABLE II. Mechanical properties of silicon, SiH, and carbon nanotubes as obtained from Tersoff-Brenner potential. (The mean diameter data relate to the equilibrium structures at zero strain.)

Tube type	Mean diameter (nm)	Poisson ratio	Critical strain (%)	Young's modulus (GPa)
(10,10) SiNT	2.205	0.279	16.23	59.36
(17,0) SiNT	2.248	0.263	15.71	57.82
(10,10) SiHNT	2.291	0.253	15.11	56.62
(17,0) SiHNT	2.334	0.243	14.87	52.47
Square SiNT	0.898	0.285	21.33	78.03
Pentagonal SiNT	0.982	0.276	20.12	71.38
Hexagonal SiNT	1.065	0.271	19.41	69.45
(10,10) CNT	1.356	0.361	29.54	988
(17,0) CNT	1.366	0.324	27.37	973

where V_0 is the equilibrium volume, ϵ is the strain, and E is the total energy.

Determining precise values of V_0 for nanotubes is extremely challenging. Hence, many current researchers generally define this volume using a shell-thickness equal to the interlayer spacing in graphite. In theory, this practice can only be extended to other forms of nanotubes if the intention is to compare their stiffnesses with that of carbon nanotubes. However, the present study judges this simplification to be acceptable for the current qualitative comparison of the mechanical behaviors of SiNTs with those of carbon nanotubes.^{28,29}

As shown in Eq. (2) below, the Poisson ratio is calculated as the negative ratio of the relative change in radius over the relative elongation, i.e.,

$$\nu = - \frac{R(\epsilon) - R_0}{R_0}, \quad (2)$$

where $R(\epsilon)$ is the tube radius at strain ϵ , and R_0 is the radius at the equilibrium (no strain).

Table II presents the calculated mechanical properties of the silicon and carbon nanotubes considered in the present study. It is noted that the Young's moduli of the SiNTs are clearly lower than those of the conventional carbon nanotubes (CNTs). This observation can be attributed to various differences in the carbon and Si bond properties. For example, the C-C bond is known to be stronger than the Si-Si bond and it is reasonable to assume that in a low-dimensional structure such as a nanotube the same property must appear.^{37,59,60} A further explanation may involve the inability of Si to form strong π bonds, thereby stabilizing sp^2 hybridization. The overlap of the p - π atomic valence orbitals for carbon is far larger than that for silicon at corresponding equilibrium distances, i.e., silicon favors sp^3 -type bonds rather than sp^2 bonds. Hence, the sp^2 -type SiNTs are significantly less stiff than the CNTs under axial tension. The discovery that at high pressures, cubic-diamond-structured silicon can undergo a phase transformation to highly coordinated metallic phases such as β -tin and hexagonal closed-packed structures was reported by Chang *et al.*⁶¹ in early 1985. Recently, Bai *et al.*⁶² presented atomistic computer-simulation evidence for three of the thinnest me-

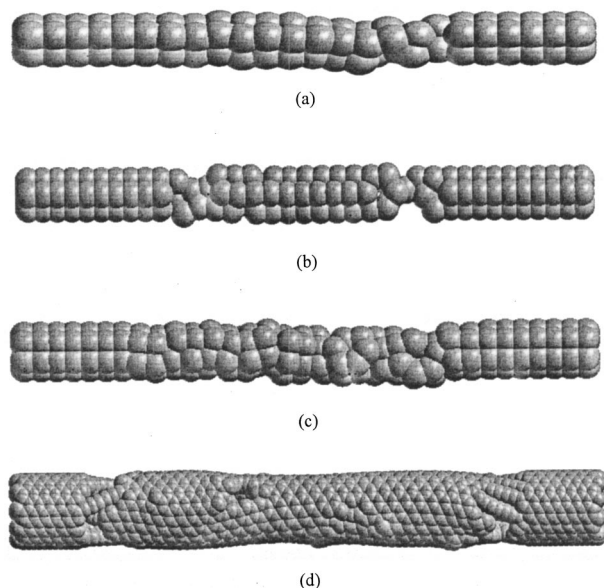


FIG. 3. Typical structural snapshots of three metallic SiNTs and carbon-nanotube-like SiNT under maximum tensile strain before plastic deformations set in. (a) Square, (b) pentagonal, (c) hexagonal metallic SiNTs, and (d) (10,10) carbon-nanotube-like SiNT.

mallic SiNTs, i.e., the square, pentagonal, and hexagonal types. The local geometric structures of these metallic SiNTs differ from that of carbon-nanotube-like SiNTs in that they are composed of sp^3 -type bonds. Table II presents the mechanical properties of these metallic SiNTs and compared the results with those for carbon-nanotube-like SiNTs and CNTs. Furthermore, the structures of these metallic SiNTs and carbon-nanotube-like SiNT under maximum tensile strains also are shown in Fig. 3. Here, the critical strains are found to be 21.33%, 20.12%, and 19.41% for the square, pentagonal, and hexagonal metallic SiNTs, respectively. The critical strains of these metallic SiNTs are significantly higher than those of carbon-nanotube-like SiNTs. Therefore, it appears that the local geometric structure alters not only the electronic properties⁶²⁻⁶⁷ but also the mechanical properties of the nanotube.

In addition, Table II indicates that the (10,10) and (17,0) SiH nanotubes have lower tensile strengths (corresponding to critical strains) than the SiNTs. Consequently, it can be concluded that the mechanical properties of the nanotubes are strongly influenced by surface hydrogen effects. Specifically, the reduction in nanotube strength may arise from the competition involved in forming hydrogen-silicon and silicon-silicon bonds under tensile loading. During tensile deformation, the hydrogen atoms are liable to “catch” some of the free silicon bonds. This prompts the formation of Si-H bonds around the tube walls, which subsequently reduces the fracture resistance of the nanotubes.

B. Effects of temperature and strain rate on silicon and Si-based nanotubes

This study assumes that since tube failure occurs as a result of dynamic processes, the mechanisms of material de-

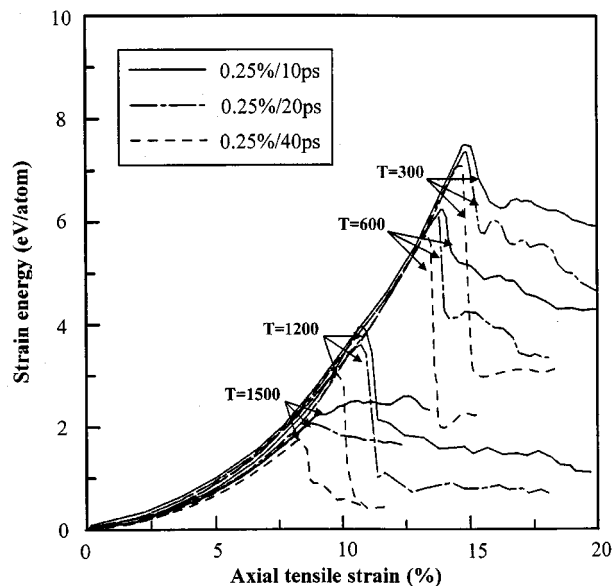
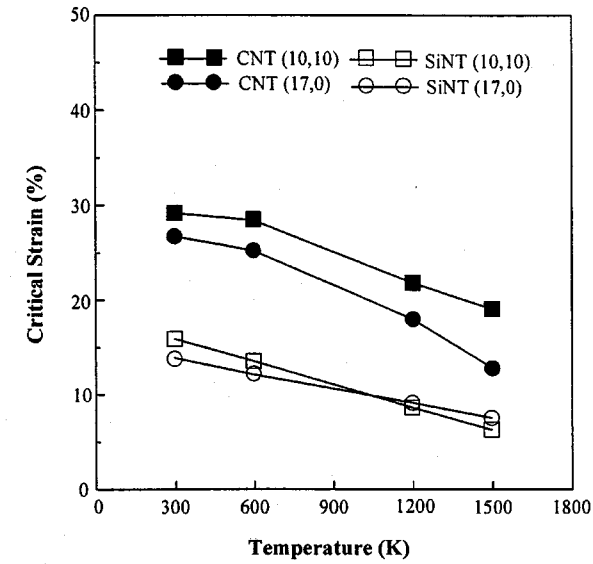
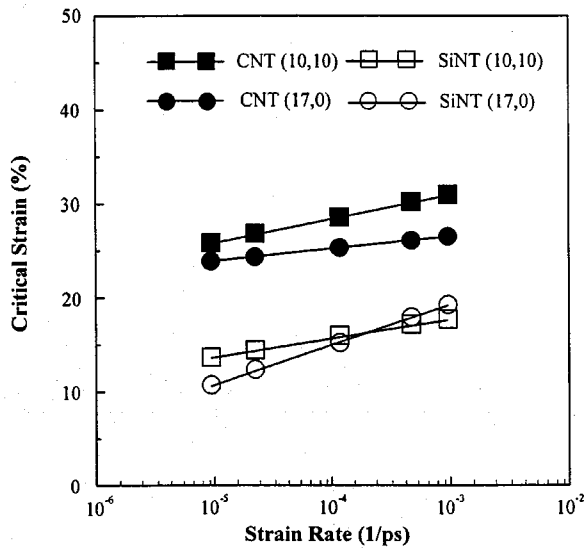


FIG. 4. Variation in strain energy with axial tensile strain for representative silicon nanotube [i.e., the (10,10) SiNT] at different temperatures and strain rates.

formation are influenced both by temperature and by strain rate. Therefore, if material deformations in silicon nanotubes are to be fully understood, the precise influences of these factors must be comprehensively investigated. Figure 4 presents the strain energies of a SiNT as a function of the tensile strain for temperatures of $T=300$ K, 600 K, 1200 K, and 1500 K and strain rates of 0.25% / 10 ps, 0.25% / 20 ps, and 0.25% / 40 ps. For reasons of clarity, the figure considers the case only of a single representative SiNT, i.e., the (10,10) SiNT. Meanwhile, Figs. 5(a) and 5(b) present the variation in critical strain with the temperature and strain rate, respectively, for the (10,10) armchair and (17,0) zigzag silicon and carbon nanotubes. The results clearly demonstrate that in all cases, the yield strain (and the corresponding tensile strength) decreases at higher temperatures and at slower strain rates. Consequently, the mechanical properties of both nanotubes are sensitive to the strain rate and temperature conditions. Regarding the strain rate influence, the strain or deformation tends not to be uniformly distributed within the material, particularly when a large strain is applied. Hence, some regions of the nanotube are subjected to larger stresses or strains than others, and it is within these regions that defects will first become evident. In the present study, when a slower strain rate is applied, the SiNTs have more time to induce adequate local deformations, and hence the onset of plastic deformation is accelerated. Therefore, in SiNTs, a slower strain rate results in a lower tensile strength under tension conditions. Considering the temperature influence, a higher temperature also results in a lower tensile strength since, as the temperature is increased, a greater number of molecules gain sufficient energy to overcome the activation energy barrier, and hence plastic deformation occurs. This result suggests that a thermally activated process plays an activating role in the complete elongation of SiNTs. However, it is also feasible that thermal effects play a “healing” role in mending broken bonds.



(a)

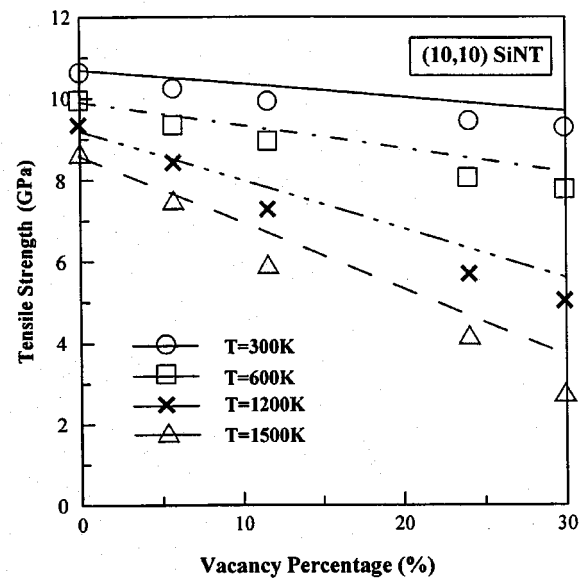


(b)

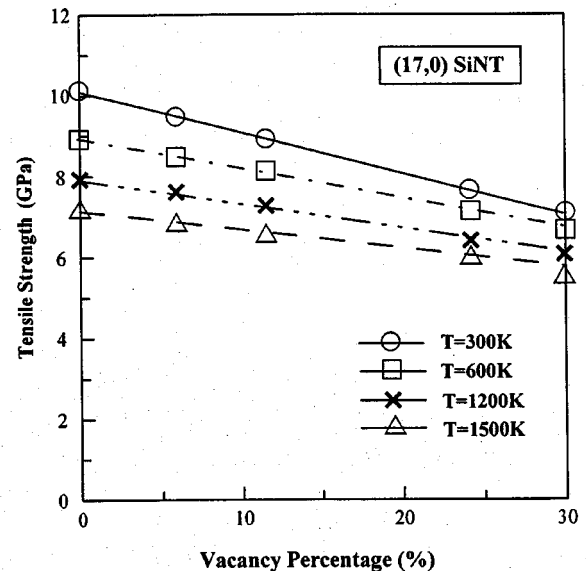
FIG. 5. (a) Variation in critical strain with temperature for silicon and carbon nanotubes at constant strain rate of 0.25% / 20 ps. (b) Variation in critical strain with strain rate for silicon and carbon nanotubes at constant temperature of $T=300$ K.

C. Effects of vacancy defects in silicon and Si-based nanotubes

This section considers the effects of various percentages (V) of randomly positioned vacancy defects upon the mechanical properties of SiNTs. The random distribution of the vacancies is modeled as follows: (i) a vacancy percentage is specified in the range of 6% to 30% and is then applied to the total number of atoms within the material to calculate the actual number of vacancies, (ii) the random vacancies are numbered sequentially, (iii) the occupation positions of the vacancies are derived, and (iv) the atoms and the vacancies are converted to their actual positions in the simulation. Tensile testing is then simulated in order to explore the effects of the vacancies on the mechanical properties of the nanotubes.



(a)



(b)

FIG. 6. Tensile strength of elongated tubes as a function of various vacancy percentages at various constant temperatures, (a) (10,10) SiNT and (b) (17,0) SiNT.

Figures 6(a) and 6(b) present the tensile strength of the elongated tubes as a function of various vacancy percentages at various constant temperatures for the (10,10) and (17,0) silicon nanotubes, respectively. It is interesting to note that at higher temperatures, there is a dramatic reduction in the absolute value of the tensile strengths of the (10,10) and (17,0) SiNTs. It is also noted that at lower temperatures, the tensile strength decreases gradually as the vacancy percentage increases. This suggests that as the temperature increases, the strained SiNTs overcome the local energy barrier and develop fragile structures, even in the case of lower vacancy percentages. In other words, the vacancy percentage

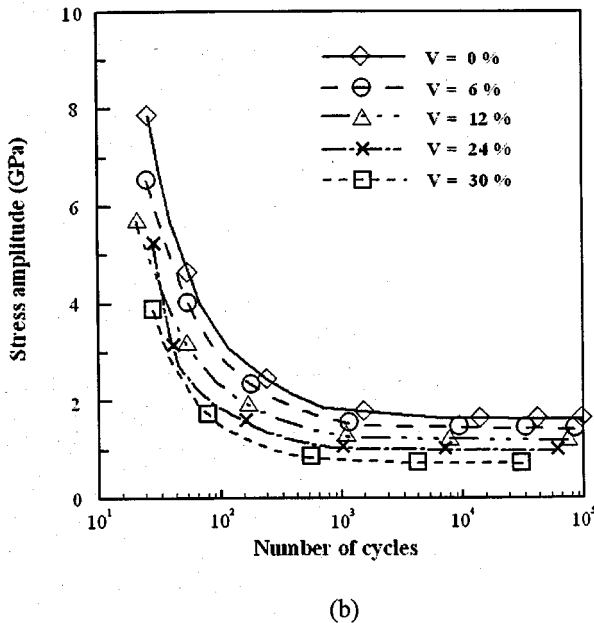
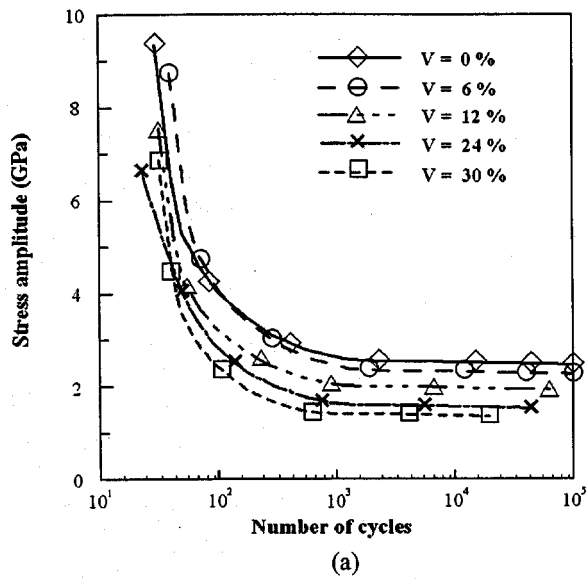


FIG. 7. Cyclic stress versus number of cycles to failure for (a) (10,10) SiNT and (b) (17,0) SiNT with various vacancy percentages and a constant temperature of $T=300\text{ K}$.

has a more significant effect upon the mechanical properties of the tubes at higher temperatures than at lower temperatures. Of the two nanotubes, it is noted that the tensile strength of the (10,10) SiNT is particularly susceptible to the presence of vacancy defects at higher temperatures.

D. Mechanical properties of silicon and Si-based nanotubes under fatigue

Figures 7(a) and 7(b) plot the variation in the stress amplitude versus the number of cycles for SiNTs with various vacancies (V) at a constant temperature of $T=300\text{ K}$, which show that the stress amplitude of the (10,10) SiNT is larger than that of the (17,0) SiNT under similar fatigue conditions.

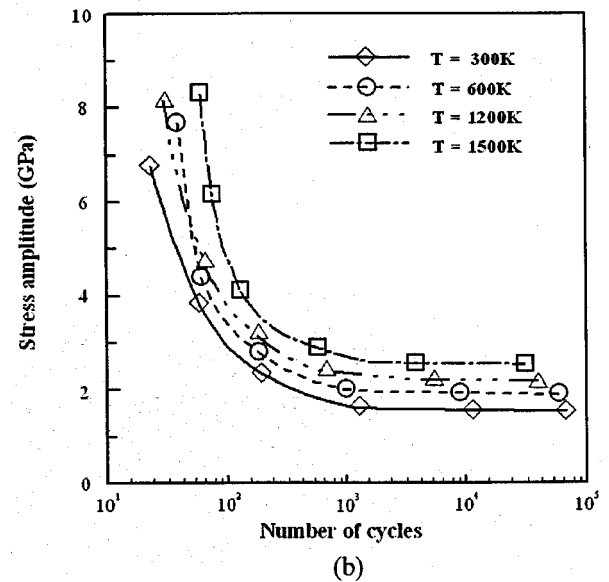
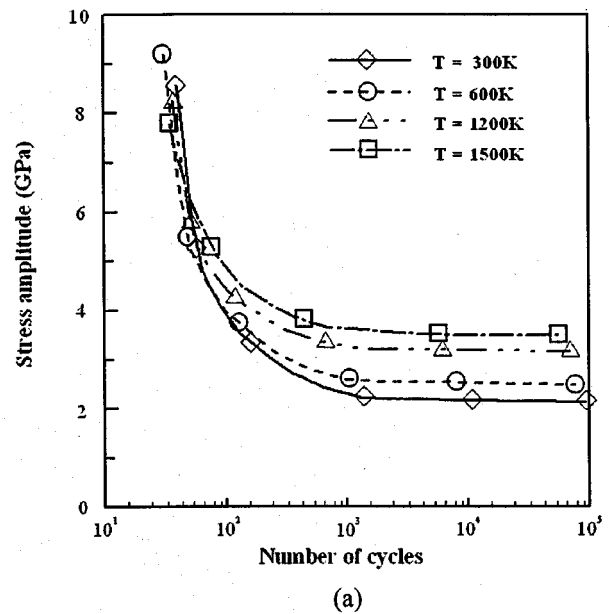


FIG. 8. Cyclic stress versus number of cycles to failure for (a) (10,10) SiNT and (b) (17,0) SiNT with $V=6\%$ and various temperatures.

In particular, the results also indicate that in the higher stress amplitude region, the effects of the vacancy percentage are not significant. However, in the lower stress amplitude region, it is clear that the stress decreases considerably as the percentage of defects increases. This observation suggests that when the value of the applied stress is less-than-critical, the lower the vacancy percentage, the higher the fatigue limit. Generally, the elongation of the material induced by increasing vacancies leads to premature yielding, thereby causing a substantial reduction in the mechanical properties of the tubes [as evidenced previously in Figs. 6(a) and 6(b)]. Figures 8(a) and 8(b) present the relationship between the stress amplitude and the number of cycles to failure at various temperatures for the (10,10) and (17,0) SiNTs with $V=6\%$. It can be seen that the fatigue stress increases with

increasing temperature. This observation is attributed to the diffusion of vacancies which occurs during cyclic loading. The diffusion phenomenon is clearly enhanced at higher temperatures. Consequently, the allowable strain, and hence the allowable stress, at a higher temperature is greater in the case of a perfect nanotube material. It is noted that the trend observed under fatigue conditions is very different from that identified under tensile testing. This difference is explained by the continuous nature of the applied stress in the tensile tests as opposed to the application of a less-than-critical applied stress in the case of the fatigue tests.

IV. CONCLUSIONS

This study has adopted the Tersoff-Brenner many-body potential to perform MD simulations of the tensile and fatigue testing of two extreme case silicon and SiH nanotubes at various temperature conditions, strain rates, and vacancy percentages. The present results validate the majority of the predictions yielded by simpler theories, and illustrate the mechanical properties and material strength limits of these nanotubes under remarkable effects, for example, various temperatures and vacancy percentages. The following con-

clusions can be drawn from the current results:

(1) The mechanical properties of bulk silicon, bulk carbon, SiNTs and CNTs have been revealed by the Tersoff-Brenner many-body potential.

(2) The tensile strength is strongly dependent on the temperature and strain rate.

(3) In general, the vacancy defect percentage has a significant influence upon the majority of the mechanical properties considered in the present study. Specifically, the mechanical properties of the nanotubes tend to reduce with increasing vacancy percentage.

(4) In the lower stress amplitude region, the fatigue limit decreases with increasing vacancy percentage. However, in the higher stress amplitude region, the vacancy percentage has no significant influence on the fatigue limit. Additionally, the fatigue stress increases with increasing temperature.

ACKNOWLEDGMENTS

The authors gratefully acknowledge the support provided to this research by the National Science Council, Taiwan, Contracts Nos. NSC93-2120-M-194-006 and NSC93-2120-M-194-003. The support of AFOSR under Contract No. F62562-03-P-0378 is also acknowledged.

*Author to whom all correspondence should be addressed. Email address: imeyrj@ccu.edu.tw

- ¹O. A. Shenderova, V. V. Zhirnov, and D. W. Brenner, *Crit. Rev. Solid State Mater. Sci.* **27**, 227 (2002).
- ²D. Qian, G. J. Wagner, W. K. Liu, and M. F. Yu, *Appl. Mech. Rev.* **55**, 495 (2002).
- ³N. G. Chopra, R. J. Luyken, K. Cherrey, M. L. Cohen, and S. G. Louie, *Science* **269**, 966 (1995).
- ⁴A. Loiseau, F. Willaime, and G. Hug, *Phys. Rev. Lett.* **76**, 4737 (1996).
- ⁵M. Terrones *et al.*, *Chem. Phys. Lett.* **257**, 576 (1996).
- ⁶K. Suenaga, C. Colliex, N. Demoncy, A. Loiseau, H. Pascard, and F. Willaime, *Science* **278**, 653 (1997).
- ⁷L. Rapoport, Y. Bilik, Y. Feldman, and M. Homyonfer, *Nature (London)* **387**, 791 (1997).
- ⁸Y. Feldman, E. Wasserman, D. J. Srolovitz, and R. Tenne, *Science* **267**, 222 (1995).
- ⁹R. Tenne, L. Margulis, M. Genut, and G. Hodes, *Nature (London)* **360**, 444 (1992).
- ¹⁰G. R. Patzke, F. Krumeich, and R. Nesper, *Angew. Chem., Int. Ed.* **41**, 2446 (2002).
- ¹¹Y. R. Hacoheh, E. Grunbaum, R. Tenne, J. Sloand, and J. L. Hutchinson, *Nature (London)* **395**, 336 (1998).
- ¹²Y. R. Hacoheh, R. Popovitz-Biro, E. Grunbaum, Y. Prior, and R. Tenne, *Adv. Mater. (Weinheim, Ger.)* **14**, 1075 (2002).
- ¹³Q. Chen, W. Zhou, G. Du, and L. M. Peng, *Adv. Mater. (Weinheim, Ger.)* **14**, 1208 (2002).
- ¹⁴C. Wu, W. Qin, G. Qin, D. Zhao, J. Zhang, S. Huang, S. Lu, H. Liu, and H. Lin, *Appl. Phys. Lett.* **82**, 520 (2003).
- ¹⁵M. Yada, M. Mihara, S. Mouri, and T. Kijima, *Adv. Mater. (Weinheim, Ger.)* **14**, 309 (2002).

- ¹⁶S. M. Lee, Y. H. Lee, Y. G. Hwang, D. Porezag, and Th. Frauenheim, *Phys. Rev. B* **60**, 7788 (1999).
- ¹⁷M. Cote, M. L. Cohen, and D. J. Chadi, *Phys. Rev. B* **58**, R4277 (1998).
- ¹⁸G. Seifert and E. Hernandez, *Chem. Phys. Lett.* **318**, 355 (2000).
- ¹⁹J. W. Kang and H. J. Hwang, *J. Phys.: Condens. Matter* **14**, 8997 (2002).
- ²⁰C. Su, H. T. Liu, and J. M. Li, *Nanotechnology* **13**, 746 (2002).
- ²¹P. Zhang and V. H. Crespi, *Phys. Rev. Lett.* **89**, 056403 (2002).
- ²²A. Bahel and M. V. Ramakrishna, *Phys. Rev. B* **51**, 13 849 (1995).
- ²³M. Menon and E. Richter, *Phys. Rev. Lett.* **83**, 792 (1999).
- ²⁴B. Marsen and K. Sattler, *Phys. Rev. B* **60**, 11 593 (1999).
- ²⁵M. Menon, A. N. Andriotis, and G. Froudakis, *Nano Lett.* **2**, 301 (2002).
- ²⁶S. B. Fagan, R. Mota, R. J. Baierle, G. Paiva, J. R. Silva, and A. J. Fazzio, *J. Mol. Struct.* **539**, 110 (2001).
- ²⁷O. Lourie, D. M. Cox, and H. D. Wagner, *Phys. Rev. Lett.* **81**, 1638 (1998).
- ²⁸B. I. Yakobson, C. J. Brabec, and J. Bernhole, *Phys. Rev. Lett.* **76**, 2511 (1996).
- ²⁹C. F. Cornwell and L. T. Wille, *Solid State Commun.* **10**, 555 (1997).
- ³⁰D. Srivastava, M. Menon, and K. Cho, *Phys. Rev. Lett.* **83**, 2973 (1999).
- ³¹T. Ozaki, Y. Iwasa, and T. Mitani, *Phys. Rev. Lett.* **84**, 1712 (2000).
- ³²J. W. Kang and H. J. Hwang, *J. Korean Phys. Soc.* **38**, 695 (2001).
- ³³J. W. Kang and H. J. Hwang, *Nanotechnology* **12**, 295 (2001).
- ³⁴E. W. Wong, P. E. Sheehan, and C. M. Lieber, *Science* **277**, 1971 (1997).

- (1997).
- ³⁵J. Tersoff, Phys. Rev. Lett. **56**, 632 (1986).
- ³⁶J. Tersoff, Phys. Rev. B **37**, 6991 (1988).
- ³⁷J. Sha, J. Niu, X. Ma, J. Xu, X. Zhang, and D. Yang, Adv. Mater. (Weinheim, Ger.) **14**, 1219 (2002).
- ³⁸J. J. Wortman and R. A. Evans, J. Appl. Phys. **36**, 153 (1965).
- ³⁹W. A. Brantley, J. Appl. Phys. **44**, 534 (1973).
- ⁴⁰Y. C. Fung, *Foundation of Solid Mechanics* (Prentice-Hall, New York, 1965).
- ⁴¹L. E. Malvern, *Introduction to the Mechanics of a Continuous Media* (Prentice-Hall, New York, 1969).
- ⁴²K. R. Virwani, A. P. Malshe, D. K. Sood, and R. G. Elliman, Appl. Phys. Lett. **84**, 3148 (2004).
- ⁴³S. Yi, S. Lee, and D. Cho, J. Korean Phys. Soc. **35**, 1106 (1999).
- ⁴⁴S. Lee, C. Cho, J. Kim, S. Park, S. Yi, J. Kim, and D. Cho, J. Micromech. Microeng. **8**, 330 (1998).
- ⁴⁵S. Lee, S. Park, J. Kim, S. Yi, and D. Cho, J. Microelectromech. Syst. **9**, 557 (2000).
- ⁴⁶M. F. Ansell, Chem. Br. **20**, 1017 (1984).
- ⁴⁷M. O'Keefe and B. G. Hyde, in *Structure and Bonding in Crystals*, edited by M. O'Keefe and A. Navrotsky (Academic, New York, 1981), Vol. 1.
- ⁴⁸R. H. Telling, C. J. Pickard, M. C. Payne, and J. E. Field, Phys. Rev. Lett. **84**, 5160 (2000).
- ⁴⁹J. Whitlock and A. L. Ruoff, Scr. Metall. **15**, 525 (1981).
- ⁵⁰A. L. Ruoff and J. Wanagel, Science **198**, 1037 (1977).
- ⁵¹J. Hu, M. Ouyang, P. Yang, and C. M. Lieber, Nature (London) **399**, 48 (1999).
- ⁵²N. Wang, Y. H. Tang, Y. F. Zhang, and C. S. Lee, Phys. Rev. B **58**, R16 024 (1998).
- ⁵³J. W. Kang and H. J. Hwang, Phys. Rev. B **64**, 014108 (2001).
- ⁵⁴J. W. Kang, K. S. Choi, K. R. Byun, and H. J. Hwang, J. Phys.: Condens. Matter **14**, 2629 (2001).
- ⁵⁵J. W. Kang, K. R. Byun, and H. J. Hwang, Phys. Rev. B **66**, 125405 (2002).
- ⁵⁶J. W. Kang, K. S. Choi, and H. J. Hwang, J. Korean Phys. Soc. **38**, 158 (2001).
- ⁵⁷J. W. Kang and H. J. Hwang, Comput. Mater. Sci. **21**, 509 (2001).
- ⁵⁸E. Lukevitz, O. Pudov, and R. Sturkovich, *Molecular structure of organosilicon compounds* ~ Ellis Horwood, Chichester, 1989.
- ⁵⁹J. Tersoff, Phys. Rev. B **39**, 5566 (1989).
- ⁶⁰J. Tersoff, Phys. Rev. B **38**, 9902 (1988).
- ⁶¹K. L. Chang and M. L. Cohen, Phys. Rev. B **31**, 7819 (1985).
- ⁶²J. Bai, X. C. Zeng, H. Tanaka, and J. Y. Zeng, Proc. Natl. Acad. Sci. U.S.A. **101**, 2664 (2004).
- ⁶³A. S. Barnard and S. P. Russo, J. Phys. Chem. B **107**, 7577 (2003).
- ⁶⁴M. Zhang, Y. H. Kan, Q. J. Zang, Z. M. Su, and R. S. Wang, Chem. Phys. Lett. **379**, 81 (2003).
- ⁶⁵R. Q. Zhang, S. T. Lee, W. K. Li, and B. K. Teo, Chem. Phys. Lett. **364**, 251 (2002).
- ⁶⁶S. B. Fagan, R. J. Baierle, R. Mota, and A. Fazzio, Phys. Rev. B **61**, 9994 (2000).
- ⁶⁷G. Seifert, T. Köhler, H. M. Urbassek, E. Hernández, and T. Frauenheim, Phys. Rev. B **63**, 193409 (2001).